Research article

Laura Mercadé*, Leopoldo L. Martín, Amadeu Griol, Daniel Navarro-Urrios and Alejandro Martínez

Microwave oscillator and frequency comb in a silicon optomechanical cavity with a full phononic bandgap

https://doi.org/10.1515/nanoph-2020-0148
Received February 27, 2020; accepted July 13, 2020; published online July 31, 2020

Abstract: Cavity optomechanics has recently emerged as a new paradigm enabling the manipulation of mechanical motion via optical fields tightly confined in deformable cavities. When driving an optomechanical (OM) crystal cavity with a laser blue-detuned with respect to the optical resonance, the mechanical motion is amplified, ultimately resulting in phonon lasing at MHz and even GHz frequencies. In this work, we show that a silicon OM crystal cavity performs as an OM microwave oscillator when pumped above the threshold for self-sustained OM oscillations. To this end, we use an OM cavity designed to have a breathing-like mechanical mode at 3.897 GHz in a full phononic bandgap. Our measurements show that the first harmonic of the detected signal displays a phase noise of ≈−100 dBc/Hz at 100 kHz. Stronger blue-detuned driving leads eventually to the formation of an OM frequency comb, whose lines are spaced by the mechanical frequency. We also measure the phase noise for higher-order harmonics and show that, unlike in Brillouin oscillators, the noise is increased as corresponding to classical harmonic mixing. Finally, we present real-time measurements of the comb waveform and show that it can be fitted to a theoretical model recently presented. Our results suggest that silicon OM cavities could be relevant processing elements in microwave photonics and optical RF processing, in particular in disciplines requiring low weight, compactness and fiber interconnection.

Keywords: microwave oscillator; optical frequency comb; optomechanical crystal cavity; phononic bandgap; silicon photonics.

1 Introduction

Cavity optomechanics addresses the interaction between light and mechanical waves confined in a cavity [1, 2]. When properly controlled, this interaction can give rise to a plethora of intriguing phenomena such as quantum ground-state cooling [3], phonon lasing [4, 5], optomechanically induced transparency [6, 7] or non-reciprocal behavior [8]. Amongst the different technological platforms implementing optomechanical (OM) cavities, their realization in planar photonic integrated circuits enables to accurately design the optical and mechanical resonances, as well as to maximize its interaction strength (given by the OM coupling rate, g_0). This has led to OM cavities lithographically defined on released high-index nanobeams – the so-called OM crystals [9] – with mechanical frequencies reaching up to several GHz.

Since the mechanical vibration can efficiently modulate the intensity of an input optical signal, OM cavities could play a role in microwave photonics, a discipline that addresses the processing of microwave signals in the optical domain [10]. In this sense, some experiments have shown the performance of OM cavities as radio frequency (RF) down-converters [11] or OM oscillators [12], which are essential functionalities in microwave photonics. Moreover, since OM cavities are nonlinear elements, multiple harmonics of the fundamental mechanical vibrations can be over-imposed on the optical signal [11, 13, 14], a phenomenon that has been recently interpreted theoretically

***Corresponding author: Laura Mercadé**, Nanophotonics Technology Center, Universitat Politècnica de València, Camino de Vera s/n, 46022 Valencia, Spain, E-mail: laumermo@ntc.upv.es
Leopoldo L. Martín, Nanophotonics Technology Center, Universitat Politècnica de València, Camino de Vera s/n, 46022 Valencia, Spain; and Departamento de Física, Universidad de La Laguna, Apdo. 456. E-38200, San Cristóbal de La Laguna, Santa Cruz de Tenerife, Spain
Amadeu Griol and Alejandro Martínez, Nanophotonics Technology Center, Universitat Politècnica de València, Camino de Vera s/n, 46022 Valencia, Spain. https://orcid.org/0000-0001-5448-0140 (A. Martínez)
Daniel Navarro-Urrios, MIND-IN2UB, Departament d'Enginyeria Electrònica i Biomèdica, Facultat de Física, Universitat de Barcelona, Martí i Franquès 1, 08028 Barcelona, Spain

as an optical frequency comb (OFC) [15]. Notably, recent experiments have also shown that OFCs generated by Kerr nonlinearities could also play a role in the processing of microwave signals in the optical domain [16].

In this work, we first demonstrate an OM cavity on a silicon nanobeam having a breathing mechanical mode vibrating close to 4 GHz with a high g_0 and placed in a full phononic bandgap. Then, by driving the cavity with a blue-detuned laser we demonstrate phonon lasing of this fundamental mechanical mode. We measure the phase noise of the generated microwave tone and show that the cavity can perform as an OM microwave oscillator. Stronger pumping of the cavity leads to the generation of a series of harmonics forming an OFC whose phase noise degrades with the harmonic number as in standard harmonic mixing. We also perform real-time measurements of the temporal traces that show a good agreement with a theoretical model of an OFC. This confirms that OM cavities can be used for the generation of OFCs with GHz-scale line spacing and may find application as ultracompact and lightweight processing elements for microwave photonics.

2 A one-dimensional (1D) OM crystal cavity with a full phononic bandgap

OM crystal cavities can be created on suspended silicon nanobeams with one-dimensional (1D) periodicity. The key idea is to have OM mirrors (that prevent leakage of both photons and phonons) on each nanobeam side whilst the main parameters of the periodic structure (such as the period or the size of the holes) are adiabatically changed toward its center to allocate confined modes. Moreover, the cavity has to be designed to ensure a good overlap between the optical and mechanical resonant modes to produce a sufficiently large g_0.

One of the most popular 1D OM cavities in silicon nanobeams [17] consists of a series of elliptic holes whose size and axial ratio is adiabatically modulated. This OM cavity exhibits values of $g_0/2\pi \approx 1$ MHz but it does not have a full phononic bandgap but a partial one because a full phononic bandgap cannot be obtained by merely drilling holes in the nanobeam [18]. In order to reduce phonon leakage, the cavity can be surrounded by a two-dimensional (2D) "acoustic shield", which is basically a 2D structure exhibiting a complete phononic bandgap at the required frequency [17]. This hybrid 1D/2D approach has been successfully applied in a number of experiments, such as the exploration of nonlinear dynamics [19], the cooling down to the quantum ground-state [3, 20], the phonon guidance through waveguides [21] and, more recently, the demonstration of ultrahigh mechanical quality factors $Q_m \approx 10^{10}$ in cryogenic environments [22].

Having a full phononic bandgap in a 1D silicon nanobeam requires making lateral corrugations in addition to the holes [18]. Using this approach, the existence of mechanical modes in a full phononic bandgap of a 1D OM crystal consisting of circular holes and lateral wings was demonstrated [23]. However, the mechanical modes within the bandgap in the cavity demonstrated in a study by Gomis-Bresco et al. [23] exhibit low $g_0/2\pi$ values, being the breathing mechanical mode located out of the phononic bandgap. As a result, the excitation of these modes is not efficient and, in general, all injected energy goes to the nanobeam flexural modes (oscillating at tens of MHz), which has been successfully used to demonstrate phonon lasing [24], chaotic dynamics [25] and, more recently, synchronization [26]. This basic OM structure can be further engineered so that breathing-like mechanical modes appear within the full bandgap, as shown in a study by Oudich [27]. Figure 1a and b shows, respectively, the photonic and phononic band diagrams for the mirror unit cell used to build the structure, where a dashed line has been used to mark out the position of the confined optical and mechanical modes. The unit cell (depicted in the inset of Figure 1a) can be designed to have an OM mirror that gives rise simultaneously to a TE-like photonic bandgap (Figure 1a) and a full phononic bandgap (Figure 1b). The different band colors in Figure 1b represent the different symmetry (even [E] or odd [O]) bands as a function of the Y or Z symmetry plane. Figure 1c represents the lattice parameters of the adiabatically tapered cavity, which allocates confined optical and mechanical modes (Figure 1d). The theoretical mechanical mode is found at $\Omega_m/2\pi$ = 3.82 GHz and the optical mode at $\lambda_r \approx 1530$ nm. This means that the mechanical breathing mode is inside a full phononic bandgap (dashed black line in Figure 1b). Remarkably, the calculated OM coupling rate is $g_0/2\pi \approx 540$ kHz, much higher than in the case of the mechanical modes with frequencies within the phononic bandagp observed in a study by Gomis-Bresco et al. [23].

A set of OM cavities was fabricated following the design summarized in Figure 1. Because of fabrication imperfections, the fabricated structures were a bit different from the nominal ones. Regarding the mechanical properties, fabrication imperfections may eventually lead to structures in which the mechanical breathing mode is no longer confined within the mechanical bandgap. To determine whether the fabricated structures also displayed a full phononic bandgap, we simulated numerically an OM

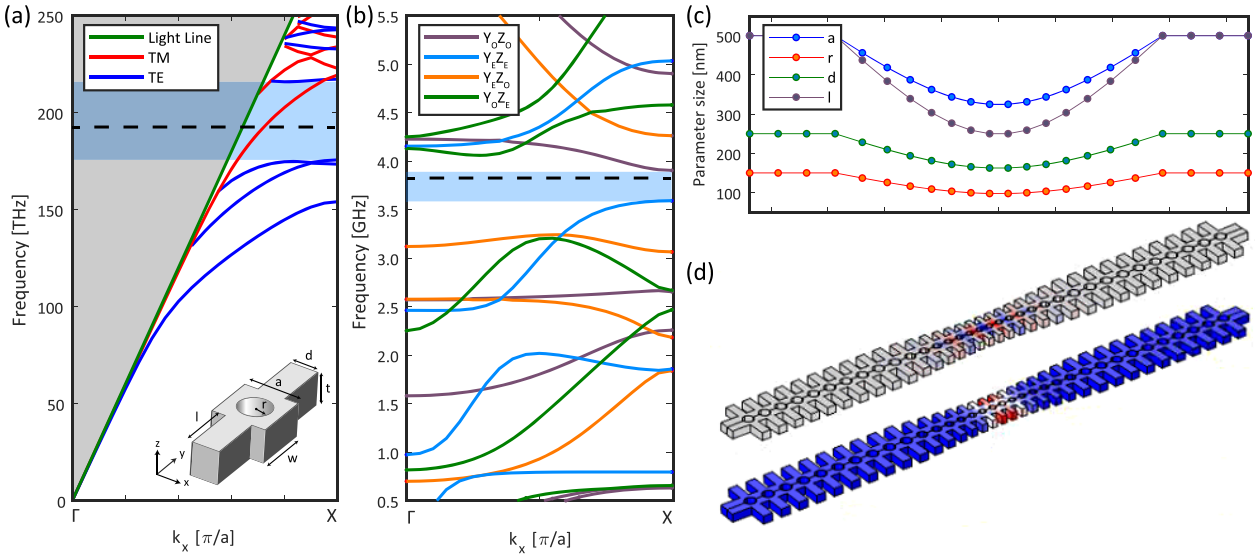

Figure 1: Design of a one-dimensional (1D) optomechanical (OM) crystal cavity with a full phononic bandgap.
(a) Photonic bands for transverse electric (TE-like) modes and transverse magnetic (TM-like) modes for the mirror unit cell. The gray- and light-blue-shaded areas denote the non-guided modes and the TE-like quasi-bandgap, respectively. (b) Phononic bands for mechanical modes with different symmetries for the mirror unit cell. (c) Parameter variation to build the OM cavity for the nominal structure. (d) Optical resonance at $\lambda_r = 1530$ nm and mechanical resonance at $\Omega_m/2\pi = 3.82$ GHz (dashed black line in (b)). The calculated OM coupling rate is $g_0/2\pi \simeq 540$ kHz. The nominal parameters are waveguide width $w = 570$ nm, and thickness $t = 220$ nm, stub mirror (defect) width $l = 500$ nm (250 nm), stub mirror (defect) length $d = 250$ nm (163 nm), hole mirror (defect) radius $r = 150$ nm (98 nm) and mirror (defect) period $a = 500$ nm (325 nm). Simulations in (a) and (b) were performed with COMSOL.

cavity using the exact dimensions retrieved from scanning electron microscope (SEM) images, as that shown in Figure 2a. This was done by using a software that enabled us to convert the SEM image into a COMSOL schematic with the unit cell shown in Figure 2d. We simulated different unit cells in the mirror region of the cavity, and the final phononic band diagram is presented in Figure 2c. It can be seen that the full mechanical bandgap remains in the fabricated sample. We also simulated numerically the optical properties of the fabricated sample and obtained an optical mode well localized in the defect region and having an intrinsic optical Q factor $Q_i = 5.9 \times 10^4$, as seen in Figure 2b.

Experimental measurements were performed at room temperature and at atmospheric pressure by coupling the light into and out of the cavity with a micro-loop fiber taper (see Supplementary material). Regarding the optical properties, the tested unheated OM cavity had an optical resonance at $\lambda_r = (1522.5 \pm 0.3)$ nm showing a loaded optical quality factor of $Q_o = 5 \times 10^3$ and an overall decay rate of $\kappa/2\pi = 39$ GHz. The experimentally transduced mechanical mode of the cavity is shown in Figure 2e and shows a resonance frequency $\Omega_m/2\pi = 3.897$ GHz with a mechanical quality factor of $Q_m = (2400 \pm 300)$, which gives a $Q_m \times f_m$ value of $(9.5 \pm 1.1) \times 10^{12}$. From Figure 2c it can be seen that the confined mechanical mode (dashed with a red line) lies inside the phononic bandgap. Therefore, we can state that this OM crystal cavity possesses a breathing mode within a mechanical bandgap and with a measured $g_0/2\pi = (660 \pm 70)$ kHz, which is of the same order of magnitude than the value calculated for the nominal cavity (see Supplementary material for more details). We also calculated the OM cooperativity, defined as $C_0 = (4g_0^2)/(\Gamma_m \kappa)$, obtaining a value $C_0 = (2.8 \pm 0.5) \times 10^{-5}$. Here, Γ_m is the measured mechanical linewidth $\Gamma_m/2\pi = (1.6 \pm 0.2)$ MHz.

3 Optomechanical microwave oscillator

High-quality microwave sources with ultra-narrow linewidths are required for a great variety of applications. Typically, microwave oscillators are made by applying frequency multiplication to an electronic source. This requires a cascade of frequency-doubling stages, which means that the power of the final signal is greatly reduced. Recently, different techniques to produce microwave tones via optical means have been proposed. The resulting device is called an optoelectronic oscillator (OEO) [28, 29].

Amongst the different techniques to build an OEO, stimulated Brillouin scattering has proven itself to be

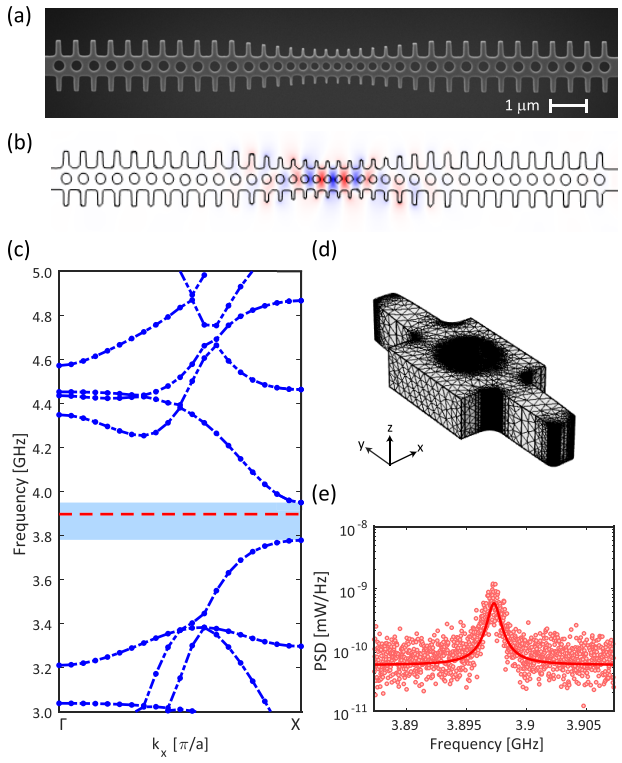

Figure 2: Optical and mechanical properties of the fabricated optomechanical (OM) cavity.
(a) Scanning electron microscope (SEM) image of the fabricated OM cavity used in the experiments; (b) field pattern of the localized optical mode in the fabricated cavity at a theoretical value of 1521.8 nm, very close to the experimental λ_r. (c) Phononic bands for the real profile mirror unit cell extracted from the SEM image, including the frequency of the experimentally observed mechanical mode, which is well confined inside the phononic bandgap; (d) unit cell considered in the phononic bands simulations in COMSOL; (e) measured power spectral density of the mechanical resonance confined in the phononic bandgap.

extremely useful since it can provide high-frequency RF signals with extreme purity (or extremely narrow linewidth). For instance, cascaded Brillouin scattering on a high-Q silica wedge cavity enabled the synthesis of a 21 GHz microwave tone with a record-low phase noise floor value of –160 dBc/Hz [30]. Owing to the equivalence between Brillouin scattering in a waveguide and OM interaction in a cavity [31], we could think that an OEO can be also obtained from an OM cavity when pumped with a blue-detuned laser source. In this case, since the involved mechanism is a self-sustained oscillation originated from OM interaction, from now on we will refer to it as an optomechanical oscillator (OMO).

In an OM crystal cavity, blue-detuned driving gives rise to a change of the mechanical frequency (the so-called optical spring effect), as well as reduction of the overall mechanical damping rate $\Gamma_{m,\mathrm{eff}} = \Gamma_m + \Gamma_{\mathrm{opt}}$ [2]. Ultimately, the threshold of instability is attained when $\Gamma_{m,\mathrm{eff}} = 0$, and the oscillator reaches the condition of self-oscillation or phonon lasing, which results in a very narrow tone in the detected spectrum at the mechanical resonance [32, 33]. Figure 3a shows the evolution of the mechanical mode frequency and linewidth when performing a laser wavelength sweep under blue-detuned driving conditions. These measurements – taken in reflection after photodetection of the signal backscattered by the OM cavity – were recorded when the thermo-optic effect shifts the optical resonance up to higher wavelengths in a typical bistability "saw-tooth" shaped transmission [32], which required a threshold power $P_{\mathrm{in}} = 2.48\,\mathrm{mW}$ reaching the fiber loop which couples to the cavity. The large pump threshold is probably due to the fact that the optical quality factor of the device previously addressed is relatively low so the device is operated in the unresolved sideband regime ($\kappa \gg \Omega_m$). Increasing the optical quality factor of the cavity should reduce this pump threshold, because, in this regime, for the optimal detuning, when $\Delta = \frac{\kappa}{2}$, $\Gamma_{\mathrm{opt}} = -8\left(\frac{g}{\kappa}\right)^2$. Here, Δ is the detuning of the laser from the optical resonance $\Delta = \omega_L - \omega_r$ and g the light-enhanced OM coupling, given by $g = g_0\sqrt{\overline{n}_{\mathrm{cav}}}$ with $\overline{n}_{\mathrm{cav}}$ the photon number circulating inside the cavity [2].

Once the mechanical resonance was self-sustained and the device entered the phonon lasing regime, we measured the phase noise of the generated microwave tone at $\Omega_m/2\pi = 3.87\,\mathrm{GHz}$, as shown in Figure 3c. The phase noise shows the typical dependencies with $1/f^3$ (flicker noise, lower part of the spectrum) and $1/f^2$ (white noise, upper part of the spectrum), which are in good agreement with the general phase noise $\mathcal{L}(f)$ described by the Leeson's model [34–36]. Future work will address a more exhaustive characterization of the different noise terms observed in the RF spectrum.

Noticeably, the phase noise becomes as low as (–100 ± 1) dBc/Hz at 100 kHz, which is a remarkable good value for a nanoscale GHz microwave oscillator. This performance is on par with some commercial mid-range devices, such as the Agilent N5183AMXG that displays a phase noise of –102 dBc/Hz at 100 kHz offset for a 10 GHz frequency [37]. In order to establish a fair comparison with other OMOs, we have calculated the equivalent phase noise at 100 kHz for a 5 GHz carrier frequency using the transformation $PN_1 = PN_0 + 20 \times \log(f_1/f_0)$. Here, PN_0 is the phase noise value at frequency f_0 of the structures to be compared and f_1 is the new equivalent carrier frequency which we have chosen to be 5 GHz. This way, we can easily compare the performance of oscillators operating at frequencies that can differ by orders of magnitude. The results

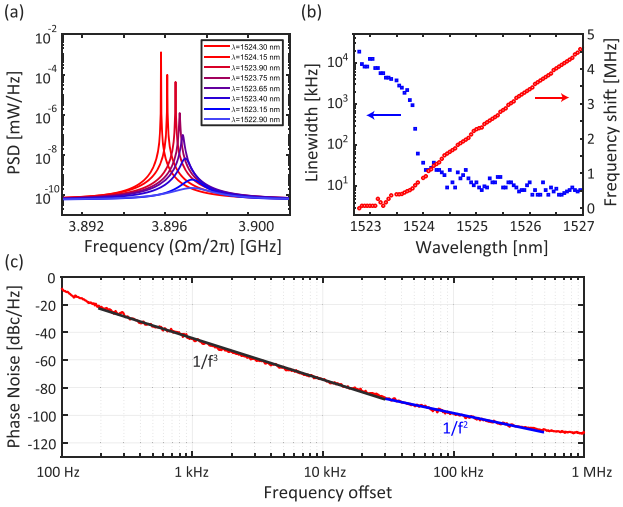

Figure 3: Driving the optomechanical (OM) crystal cavity to the phonon lasing regime at $P_{in} = 2.48$ mW.
(a) Detected RF spectra at different driving wavelengths (λ_L). (b) Evolution of the mechanical effective linewidth and the mechanical frequency as a function of λ_L for a driving power $P_{in} = 2.48$ mW. (c) Phase noise of the generated microwave tone in red and fit to $1/f^3$ and $1/f^2$ lines as described by the Lesson's model. The phase noise at 100 kHz is (−100 ± 1) dBc/Hz.

of equivalent phase noise PN_1 are summarized in Table 1. Importantly, our device improves the noise performance of silicon disks fabricated in micro-electro-mechanical systems (MEMS) technology [38]. The OMO reported in a study by Ghorbel et al. [12], which makes use of a 1D OM crystal cavity in GaAs, shows a phase noise at 100 kHz more than 10 dB worse that our device for a similar microwave frequency. Since both OM cavities display similar mechanical Q factors at room temperature (limited by material losses), the better performance of our device in terms of phase noise may be due to an improved value of g_0 or a higher driving power. On the other hand, Brillouin-based OMOs show a better performance than OM crystal cavities (phase noise around −110 dBc/Hz at $f_{RF} = 21.7$ GHz) as a result of the ultrahigh optical quality factor but at the expenses of a larger cavity foot-print ($\gg$mm^2) [30]. Therefore, with the advantages of extreme compactness and Si-technology compatibility, our approach is a very promising candidate to build ultracompact OMOs.

4 OM frequency comb

At even higher driving powers, and always operating with the laser blue-detuned with respect to the optical resonance, higher-order harmonics can be observed in the detected signal. The underlying process is similar to cascaded Brillouin scattering in an optical waveguide [40]: the Stokes and anti-Stokes photons (resulting from photon–phonon scattering from the laser source) become new pump signals that generate new Stokes and anti-Stokes photons via photon–phonon interaction, and the process is repeated over and over as long as the resulting photons can propagate in the medium (Figure 4a). This process can become extremely efficient in an optical cavity supporting both optical and mechanical whispery-gallery modes (WGMs) if the mechanical frequency equals the free-spectral range [30]. In this case, there is a strong resemblance with the formation of OFCs in traveling-wave cavities as a result of third-order nonlinear interaction: the large density of states at resonant frequencies gives rise to a set of equidistant frequency lines at the output (Figure 4b).

The generation of multiple harmonics in an OM cavity operated in the unresolved sideband regime inherits features of both effects (Figure 4c). First, the cavity linewidth is not so broad as in the case of the waveguide, but the high density of states around the resonant frequency benefits the underlying OM interaction. In comparison with the WGM cavity, the OM cavity do not support multiple optical modes exactly spaced by the mechanical frequency, which greatly relaxes the conditions to get multiple harmonics. This way, in the output optical spectrum we expect a series of peaks at frequencies $\omega_L + m\omega_m$, with amplitudes A_m, being m an integer number and ω_L the laser frequency. This closely resembles OFCs of OM nature, which has been recently

Table 1: Comparison of the phase noise of different OMOs.

References	Structure	f_{RF} (GHz)	Phase noise at 100 kHz (in dBc/Hz)	Foot-print	Equivalent phase noise at 5 GHz
[35]	SiN ring resonator	0.042	−120	≈1 mm^2	−78
[12]	1D III/V OM photonic crystal cavity	2.92	−87	<10 µm^2	−83
[39]	Si 2D photonic crystal cavity	0.112	−125	<10 µm^2	−92
[38]	MEMS oscillator	1.12	−107	≫µm^2	−94
This work	1D Si OM photonic crystal cavity	3.87	−100	<10 µm^2	−97
[30]	Silica disk	21.7	−110	≫mm^2	−122

OM, optomechanical; 1D, one-dimensional; 2D, two-dimensional; OMO, optomechanical oscillator.

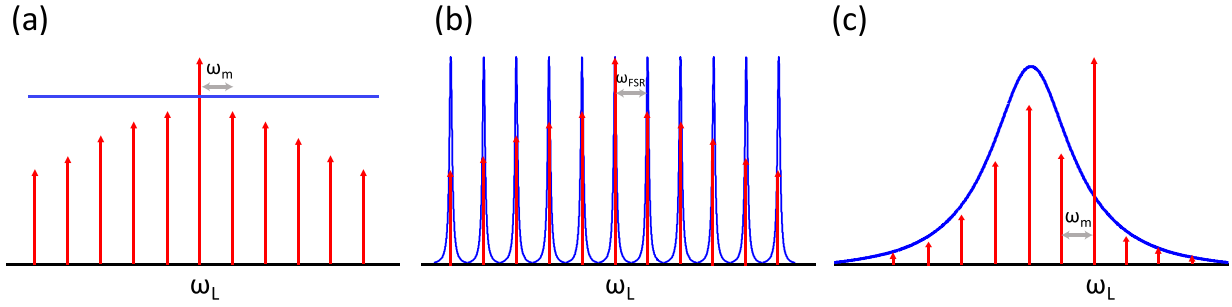

Figure 4: Generation of harmonics and optical frequency combs (OFCs) in photonic structures.
(a) In an optical waveguide, a cascaded Brillouin process gives rise to a set of harmonics spaced ω_m between them; (b) in a traveling-wave resonator supporting a series of high-Q whispery-gallery modes (WGMs) with a Kerr non-linearity, a set of harmonics is generated via four-wave mixing with a spacing ω_{FSR} from the laser frequency, where ω_{FSR} corresponds to the free-spectral range (FSR) of the resonator; (c) in an OM cavity, OM interaction induced by a blue-detuned laser scatters photons at frequencies ω_m apart from the laser frequency, which in a cascaded process generated more photons, giving rise to a series of harmonics, and ultimately to OFCs occupying the cavity optical linewidth. In the figure, the blue curves stand for the photonic response of the structure and the red arrows show the different harmonics.

analyzed theoretically in [15]. Notice that, as in the case of OFC based on the Kerr-effect in traveling-wave optical resonators [41, 42] (Figure 4b), here it is also a third-order nonlinear process what mediates in the OFC generation.

Since all generated photons are resonant within the same optical mode (Figure 4c), the number of optical carriers forming the OFC is limited by the linewidth of the optical resonance. As suggested in a study by Miri et al. [15], a cavity in the unresolved sideband regime should therefore provide wider OFCs than a cavity operating in the sideband-resolved regime. OM-generated OFCs have been previously observed using MHz-scale mechanical modes [25, 35, 39, 43]. In this case, a high-Q cavity with a bandwidth ≈1 GHz ($Q > 10^5$) can perfectly allocate a large number of harmonics. However, if we want to build an OFC from a GHz-scale fundamental harmonic, the Q factor of the cavity should be reduced to allow the build-up of a sufficient number of harmonics. In our case, the measured loaded optical Q factor, which satisfies the criteria in a study by Miri et al. [15] to produce an OM–OFC with a spacing equal to $\Omega_m/2\pi$.

To perform the experiment, we blue-detuned our laser and recorded the detected RF spectra under different input powers. For an input power of $P_{in} = 3.38$ mW, we reach the threshold for the phonon lasing, when $\lambda_L = 1543.35$ nm. When the laser wavelength in increase until $\lambda_L = 1544.37$ nm, higher-order harmonics are generated, thus resulting in an OFC, whose first five harmonics are shown in Figure 5b. Here, we show up to the fifth harmonic, but higher harmonics can be reached (see Supplementary material). Notice that going from the phonon lasing to the OFC regime requires not only an increase of the input power but also a larger wavelength of the driving laser because of the red-shift of the optical resonance because of the thermo-optic effect. Figure 5c shows the optical spectrum of the generated OFC. The width of the peaks observed in the optical spectrum is limited by the resolution of the optical spectrum analyzer, which is 0.01 nm (1.2 GHz). When photodetected, the optical peaks are beaten resulting in the multiple peaks as seen in Figure 5b. Notice that every peak results from the addition of several beats. For instance, the peak at $2\Omega_m$ results from summing up the beating notes $\omega_L + 2\Omega_m$ with ω_L, $\omega_L - 2\Omega_m$ with ω_L, $\omega_L + \Omega_m$ with $\omega_L - \Omega_m$, and all the other optical peaks that are spaced exactly that frequency. However, for any frequency, the terms including a beating of ω_L will dominate.

We also measured the phase noise of the different harmonics, as shown in Figure 5d. In principle, the harmonic mixing process will result in an added phase noise of $20 \times \log(m)$ with respect to that of the first harmonic. It can be seen that the previous rule is well satisfied in our device. Notice that this is in stark contrast with the Brillouin OMO in high-Q cavities, for which higher harmonics show a better noise performance because the Brillouin process purifies the laser beam [30]. This is because the device in a study by Jiang et al. [30] operates in the regime where the photon lifetime exceeds the phonon lifetime in the cavity, which results in a narrowing of the Stokes line [44]. In our case, we operate in the opposite scenario, being optical losses larger than mechanical losses so the scattered Stokes wave is essentially a frequency-shifted copy of the laser beam plus an extra phase noise added by the mechanical oscillator [44]. Thus, the cavity acts as a harmonic generator (comb) and the phase noise behaves as in a conventional harmonic mixer, being the phase noise impaired by the factor previously mentioned.

In addition, we studied the optical traces of the generated OFC in the time domain. The dynamics of OM frequency

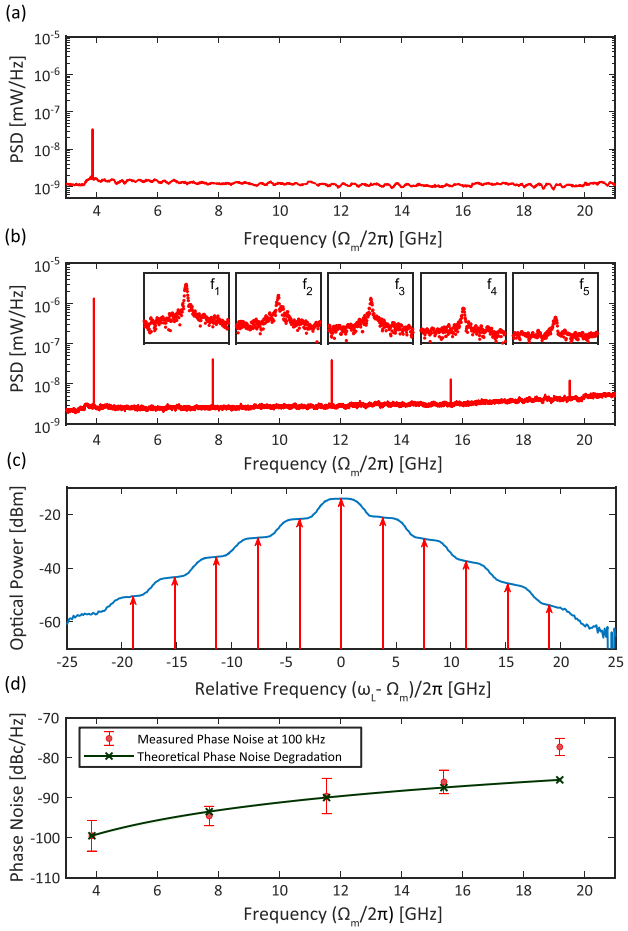

Figure 5: Optical frequency comb (OFC) generation in the OM crystal cavity at P_{in} = 3.38 mW.
(a) Detected RF spectrum above the phonon lasing threshold at λ_L = 1543.35 nm; (b) RF spectrum at λ_L = 1544.37 nm where the OFC is produced. Five harmonics are observed, being higher-harmonic tones obscured by the thermal noise of the detection system. Close views of the five harmonics within a span of 200 MHz are shown as insets; (c) recorded optical spectrum (in blue) showing a set of peaks corresponding to different harmonics represented (in red) at the expected position. (d) Phase noise of the different harmonics of the OFC. In red, the mean value of the phase noise for different phase noise measurements is presented with its standard error and in green. The theoretical phase noise degradation of 20 × log (m) with respect to that of the first harmonic is also shown.

combs can be described by the next set of coupled equations describing the time evolution of the optical mode amplitude a and the amplitude of motion x as [2, 15]:

$$\frac{da}{dt} - \left(i(\Delta + Gx) - \frac{\kappa}{2}\right)a = \sqrt{\kappa_e}s_{in} \quad (1)$$

$$\frac{d^2x}{dt^2} + \Gamma_m\frac{dx}{dt} + \Omega_m^2 x = \frac{\hbar G}{m_{eff}}|a|^2 \quad (2)$$

where Δ is the detuning of the laser from the optical resonance, G is the optical frequency shift per displacement unit, κ is the overall intensity decay rate, κ_e represents the input coupling losses, s_{in} is the input photon flux and m_{eff} is the effective mass of the mechanical oscillator. In the blue-detuned regime ($\Delta = \omega_L - \omega_r > 0$) the OM damping rate Γ_{opt} becomes negative, decreasing the overall damping rate $\Gamma_{m,eff}$ that first leads to heating of the oscillator. When the overall damping rate finally becomes negative, an instability appears producing an exponential grown of any fluctuation, which will finally saturate by nonlinear effects giving rise to a phonon lasing regime [2]. The saturation of these self-induced oscillations can be seen in Figure 6a which was obtained from the numerical simulations of the OM coupled equations (1) and (2). A close view on the saturated regime is shown in Figure 6b.

The experimental traces were acquired by photodetecting the transmitted optical signal via a high-speed and high-sensitivity photoreceiver whilst the reflected signal was used to trigger the waveform in a high-speed oscilloscope (for more details about the experimental setup see Supplementary material). Both, the theoretical and experimental temporal traces are presented in Figure 7 for different laser wavelengths – corresponding to different detunings – and input photon fluxes $|s_{in}|^2$ – placed between 0.9×10^{17} s^{-1} and 1.7×10^{17} s^{-1}. These input photon fluxes, defined as the rate of photons arriving to the cavity, are related to the input powers presented before as $P_{in} = \hbar\omega_L|s_{in}|^2$ [2]. It has to be noted that, despite the wavelength resonance was originally placed at 1522.5 nm, we were able to shift it up to values as higher as 1550 nm, as in the recorded traces reported here, due to the thermo-optic effect [32]. This effect causes a typical bistability "saw-tooth" shaped transmission, which gets both broader and shallower when the input power is increased [45]. In this regime, it is impossible to know accurately the position of the optical resonance, and, as a result, we cannot know the optical detuning Δ. Because of that, the detuning, shown in the temporal traces of Figure 7, has been set as a fit

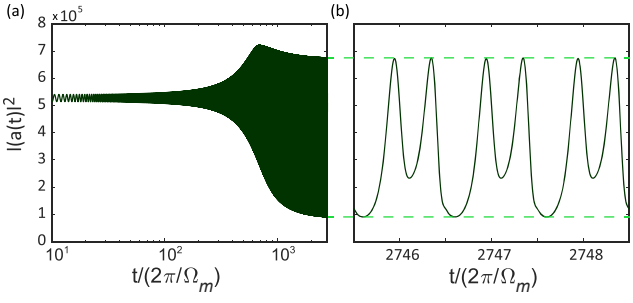

Figure 6: (a) Simulated self-induced oscillations showing the evolution of the intracavity photons versus time in logarithmic scale. (b) Close view of the saturated oscillation with a stable amplitude corresponding to the optical traces of the optical frequency comb (OFC).

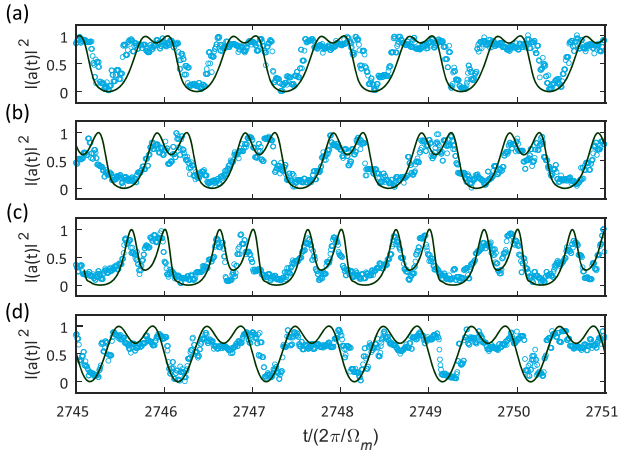

Figure 7: Comparison of the experimental (blue dots) and theoretical (solid line) temporal optomechanical (OM)-generated optical frequency comb (OFC) traces under different experimental conditions.
(a) λ_L = 1543.35 nm (experiment) and $\Delta = 4\Omega_m$ (simulation);
(b) λ_L = 1544.05 nm (experiment) and $\Delta = 3.4\Omega_m$ (simulation);
(c) λ_L = 1545.37 nm (experiment) and $\Delta = 2.4\Omega_m$ (simulation);
(d) λ_L = 1545.62 nm (experiment) and $\Delta = \Omega_m$ (simulation).

parameter in order to compare the theoretical and experimental optical traces.

The remaining cavity parameters required in the theoretical model were obtained from the simulation of the fabricated structure. In particular, we used a mechanical zero-point fluctuation amplitude $Xzpf = 2.69 \times 10^{-15}$ m and $m_{\text{eff}} = 2.7 \times 10^{-16}$ kg, obtained from the OM crystal cavity simulations. For the overall decay rate, we introduced the experimental measurements of $\kappa/2\pi = 39$ GHz and $\kappa_e = 0.26\kappa$. Figure 7 shows a nice agreement between the experiments and the theoretical model. Different waveforms can be obtained by modifying either the detuning or the input power, as pointed out in a study by Miri [15]. We also observed different waveforms (not shown here) for other driving conditions, being highly reproducible using the theoretical model. This confirms that OM cavities can be used to synthetize microwave waveforms beyond the generation of single microwave tones and, therefore, they can play a role in the development of microwave photonics applications in silicon photonics technology.

5 Conclusions

In summary, we have demonstrated a novel silicon OM crystal cavity that exhibits a large OM coupling rate for a GHz mode within a full phononic bandgap. We have shown that this OM cavity can perform as an ultracompact OMO at a microwave frequency around 4 GHz working at room temperature. Notice that our device is a free-running or open-loop OMO: the device generates an RF tone and there is no any feedback loop to improve the frequency stabilization. Operating at cryogenic temperatures would enormously improve the phase noise [46] as a result of the enhancement of the mechanical Q factor because of the full phononic bandgap [22]. This would also allow us to discern if the phononic bandgap plays a role in the better performance in terms of phase noise in comparison to the OM crystal reported in a study by Ghorbel et al. [12]. Tunability of the resulting microwave signal could be achieved by injection locking to an external optically modulated tone [47]. In addition, the preliminary demonstration of the OFC paves the way toward synthesis of microwave signals beyond the generation of pure continuous wave tones. The main advantages of the OM cavity approach for RF and microwave signal processing are its extreme compactness and low weight, highly desirable in space and satellite applications, as well as its compatibility with silicon electronics and photonics technology. The resulting optomechanically generated OFC could also be useful in sensing and spectroscopy applications by taking profit of the small distance between comb lines which would enable detection using standard electronic equipment. We also envisage that this new OM cavity could be useful in quantum applications since the mechanical Q factor can be extremely increased in cryogenic environments [48].

Acknowledgment: The authors thank Borja Vidal and Miguel A. Piqueras for technical support. L. M. would like to thank M.-A. Miri for helpful comments.
Author contribution: All the authors have accepted responsibility for the entire content of this submitted manuscript and approved submission.
Research funding: This work was supported by the European Commission (PHENOMEN H2020-EU-713450); Programa de Ayudas de Investigación y Desarrolo (PAID-01-16) de la Universitat Politècnica de València; Ministerio de Ciencia, Innovación y Universidades (PGC2018-094490-B, PRX18/00126) and Generalitat Valenciana (PROMETEO/2019/123, PPC/2018/002, IDIFEDER/2018/033).
Conflict of interest statement: The authors declare no conflicts of interest regarding this article.

References

[1] T. J. Kippenberg and K. J. Vahala, "Cavity optomechanics: back-action at the mesoscale," *Science*, vol. 321, no. 5893, pp. 1172–1176, 2008.

[2] M. Aspelmeyer, T. J. Kippenberg, and F. Marquardt, "Cavity optomechanics," *Rev. Mod. Phys.*, vol. 86, no. 4, pp. 1391–1452, 2014.
[3] J. Chan, T. P. Alegre, A. H. Safavi-Naeini, et al., "Laser cooling of a nanomechanical oscillator into its quantum ground state," *Nature*, vol. 478, no. 7367, pp. 89–92, 2011.
[4] I. S. Grudinin, A. B. Matsko, and L. Maleki, "Brillouin lasing with a CaF_2 whispering gallery mode resonator," *Phys. Rev. Lett.*, vol. 102, no. 4, p. 043902, 2009.
[5] I. S. Grudinin, H. Lee, O. Painter, and K. J. Vahala, "Phonon laser action in a tunable two-level system," *Phys. Rev. Lett.*, vol. 104, no. 8, p. 083901, 2010.
[6] S. Weis, R. Rivière, S. Deléglise, et al., "Optomechanically induced transparency," *Science*, vol. 330, no. 6010, pp. 1520–1523, 2010.
[7] A. H. Safavi-Naeini, T. P. Mayer Alegre, J. Chan, et al., "Electromagnetically induced transparency and slow light with optomechanics," *Nature*, vol. 472, no. 7341, pp. 69–73, 2011.
[8] F. Ruesink, M. A. Miri, A. Alù, and E. Verhagen, "Nonreciprocity and magnetic-free isolation based on optomechanical interactions," *Nat. Commun.*, vol. 7, no. 1, p. 13662, 2016.
[9] M. Eichenfield, J. Chan, R. M. Camacho, K. J. Vahala, and O. Painter, "Optomechanical crystals," *Nature*, vol. 462, no. 7269, pp. 78–82, 2009.
[10] J. Capmany and D. Novak, "Microwave photonics combines two worlds," *Nat. Photon.*, vol. 1, no. 6, pp. 319–330, 2007.
[11] M. Hossein-Zadeh and K. J. Vahala, "Photonic RF down-converter based on optomechanical oscillation," *IEEE Photon. Technol. Lett.*, vol. 20, no. 4, pp. 234–236, 2008.
[12] I. Ghorbel, R. Zhu, D. Dolfi, et al., "Optomechanical gigahertz oscillator made of a two photon absorption free piezoelectric III/V semiconductor," *APL Photon.*, vol. 4, no. 11, p. 116103, 2019.
[13] T. J. Kippenberg, H. Rokhsari, T. Carmon, A. Scherer, and K. J. Vahala, "Analysis of radiation-pressure induced mechanical oscillation of an optical microcavity," *Phys. Rev. Lett.*, vol. 95, no. 3, p. 033901, 2005.
[14] T. Carmon, H. Rokhsari, L. Yang, T. J. Kippenberg, and K. J. Vahala, "Temporal behavior of radiation – pressure-induced vibrations of an optical microcavity phonon mode," *Phys. Rev. Lett.*, vol. 94, no. 22, p. 223902, 2005.
[15] M.-A. Miri, G. D'Aguanno, and A. Alú, "Optomechanical frequency combs," *New J. Phys.*, vol. 20, no. 4, p. 043013, 2018.
[16] V. Torres-Company and A. M. Weiner, "Optical frequency comb technology for ultra-broadband radiofrequency photonics," *Laser Photon. Rev.*, vol. 8, no. 3, pp. 368–393, 2014.
[17] J. Chan, A. H. Safavi-Naeini, J. T. Hill, S. Meenehan, and O. Painter, "Optimized optomechanical crystal cavity with acoustic radiation shield," *Appl. Phys. Lett.*, vol. 101, no. 8, p. 081115, 2012.
[18] Y. Pennec, B. Djafari Rouhani, C. Li, et al., "Band gaps and cavity modes in dual phononic and photonic strip waveguides," *AIP Adv.*, vol. 1, no. 4, p. 041901, 2011.
[19] A. G. Krause, J. T. Hill, M. Ludwig, et al., "Nonlinear radiation pressure dynamics in an optomechanical crystal," *Phys. Rev. Lett.*, vol. 115, no. 23, p. 233601, 2015.
[20] L. Qiu, I. Shomroni, P. Seidler, and T. J. Kippenberg, "High-fidelity laser cooling to the quantum ground state of a silicon nanomechanical oscillator," 2019, arXiv: 1903.10242 [quant-ph].
[21] K. Fang, M. H. Matheny, X. Luan, and O. Painter, "Optical transduction and routing of microwave phonons in cavity-optomechanical circuits," *Nat. Photon.*, vol. 10, p. 489, 2016.
[22] G. S. MacCabe, H. Ren, J. Luo, et al., "Phononic bandgap nanoacoustic cavity with ultralong phonon lifetime," 2019, arXiv: 1901.04129 [cond-mat.mes-hall].
[23] J. Gomis-Bresco, D. Navarro-Urrios, M. Oudich, et al., "A one-dimensional optomechanical crystal with a complete phononic band gap," *Nat. Commun.*, vol. 5, no. 1, p. 4452, 2014.
[24] D. Navarro-Urrios, N. E. Capuj, J. Gomis-Bresco, et al., "A self-stabilized coherent phonon source driven by optical forces," *Sci. Rep.*, vol. 5, p. 15733, 2015.
[25] D. Navarro-Urrios, N. E. Capuj, M. F. Colombano, et al., "Nonlinear dynamics and chaos in an optomechanical beam," *Nat. Commun.*, vol. 8, no. 1, p. 14965, 2017.
[26] M. F. Colombano, G. Arregui, N. E. Capuj, et al., "Synchronization of optomechanical nanobeams by mechanical interaction," *Phys. Rev. Lett.*, vol. 123, no. 1, p. 017402, 2019.
[27] M. Oudich, S. El-Jallal, Y. Pennec, et al., "Optomechanic interaction in a corrugated phoxonic nanobeam cavity," *Phys. Rev. B*, vol. 89, no. 24, p. 245122, 2014.
[28] L. Maleki, "The optoelectronic oscillator," *Nat. Photon.*, vol. 5, no. 12, pp. 728–730, 2011.
[29] X. S. Yao and L. Maleki, "Optoelectronic microwave oscillator," *J. Opt. Soc. Am. B*, vol. 13, no. 8, pp. 1725–1735, 1996.
[30] J. Li, H. Lee, and K. J. Vahala, "Microwave synthesizer using an on-chip Brillouin oscillator," *Nat. Commun.*, vol. 4, no. 1, p. 2097, 2013.
[31] R. Van Laer, R. Baets, and D. Van Thourhout, "Unifying Brillouin scattering and cavity optomechanics," *Phys. Rev. A*, vol. 93, no. 5, p. 053828, 2016.
[32] D. Navarro-Urrios, J. Gomis-Bresco, S. El-Jallal, et al., "Dynamical back-action at 5.5 GHz in a corrugated optomechanical beam," *AIP Adv.*, vol. 4, no. 12, p. 124601, 2014.
[33] F. Pan, K. Cui, G. Bai, et al., "Radiation-pressure-antidamping enhanced optomechanical spring sensing," *ACS Photon.*, vol. 5, no. 10, pp. 4164–4169, 2018.
[34] S. Tallur, S. Sridaran, S. A. Bhave, and T. Carmon, "Phase noise modeling of opto-mechanical oscillators," in *2010 IEEE International Frequency Control Symposium*, 2010, pp. 268–272.
[35] S. Tallur, S. Sridaran, and S. A. Bhave, "A monolithic radiation-pressure driven, low phase noise silicon nitride opto-mechanical oscillator," *Opt. Express*, vol. 19, no. 24, pp. 24522–24529, 2011.
[36] E. Rubiola, *Phase Noise and Frequency Stability in Oscillators. The Cambridge RF and Microwave Engineering Series*, Cambridge, England: Cambridge University Press, 2008.
[37] https://www.keysight.com/us/en/assets/7018-08250/datasheets/5989-7572.pdf.
[38] S. Sridaran and S. A. Bhave, "1.12 GHz opto-acoustic oscillator," in *2012 IEEE 25th International Conference on Micro Electro Mechanical Systems (MEMS)*, 2012, pp. 664–667.
[39] X. Luan, Y. Huang, Y. Li, et al., "An integrated low phase noise radiation-pressure-driven optomechanical oscillator chipset," *Sci. Rep.*, vol. 4, p. 6842, 2014.
[40] M. S. Kang, A. Nazarkin, A. Brenn, and P. S. J. Russell, "Tightly trapped acoustic phonons in photonic crystal fibres as highly nonlinear artificial Raman oscillators," *Nat. Phys.*, vol. 5, no. 4, pp. 276–280, 2009.
[41] P. Del'Haye, A. Schliesser, O. Arcizet, T. Wilken, R. Holzwarth, and T. J. Kippenberg, "Optical frequency comb generation from a monolithic microresonator," *Nature*, vol. 450, no. 7173, pp. 1214–1217, 2007.

[42] T. J. Kippenberg, R. Holzwarth, and S. A. Diddams, "Microresonator-based optical frequency combs," *Science*, vol. 332, no. 6029, pp. 555–559, 2011.
[43] A. A. Savchenkov, A. B. Matsko, V. S. Ilchenko, D. Seidel, and L. Maleki, "Surface acoustic wave optomechanical oscillator and frequency comb generator," *Opt. Lett.*, vol. 36, no. 17, pp. 3338–3340, 2011.
[44] A. H. Safavi-Naeini, D. Van Thourhout, R. Baets, and R. Van Laer, "Controlling phonons and photons at the wavelength scale: integrated photonics meets integrated phononics," *Optica*, vol. 6, no. 2, pp. 213–232, 2019.
[45] D. Navarro-Urrios, J. Gomis-Bresco, N. E. Capuj, et al., "Optical and mechanical mode tuning in an optomechanical crystal with light-induced thermal effects," *J. Appl. Phys.*, vol. 116, no. 9, p. 093506, 2014.
[46] M. Hossein-Zadeh and K. J. Vahala, "An optomechanical oscillator on a silicon chip," *IEEE J. Sel. Top. Quant. Electron.*, vol. 16, no. 1, pp. 276–287, 2010.
[47] M. Hossein-Zadeh and K. J. Vahala, "Observation of injection locking in an optomechanical RF oscillator," *Appl. Phys. Lett.*, vol. 93, no. 19, p. 191115, 2008.
[48] M. Mirhosseini, A. Sipahigil, M. Kalaee, and O. Painter, "Quantum transduction of optical photons from a superconducting qubit," 2020, arXiv: 2004.04838 [quant-ph].

Supplementary Material: The online version of this article offers supplementary material (https://doi.org/10.1515/nanoph-2020-0148).